

Generation of Long-Scale Magnetic Fields from Rippled Surface Irregularities

T. Yabe, Y. Kitagawa, A. Ishizaki, M. Naito, A. Nishiguchi, M. Yokoyama, and C. Yamanaka

Institute of Laser Engineering, Osaka University, Suita, Osaka 565, Japan

(Received 30 August 1983)

A mechanism of long-scale magnetic field generation from rippled surface irregularities is given and compared with the thermoelectric effect. Criteria are given for the former dominating over the latter. These criteria are accessible in present-day experiments. An experiment is done to show an implication of the above mechanism.

PACS numbers: 52.50.Jm, 47.65.+a, 52.30.+r

Uniform compression of a spherical target is one of the key issues for inertial confinement fusion. There are many obstacles to uniform compression, such as nonuniform laser illumination,^{1,2} surface roughness of the target, the Rayleigh-Taylor instability,^{3,4} the converging amplification instability,^{5,6} and so forth. Furthermore, large-scale magnetic fields induced by various mechanisms degrade the uniform compression by causing electron flux bunching⁷ and so on. Although various mechanisms have been proposed for magnetic field generation, the simplest one, such as $\nabla T \times \nabla n$,⁸ may be the most dangerous source. When the spot size L of a laser beam becomes large, this source decreases in proportion to L^{-2} and is believed to become less of a problem. This argument is not correct in an exact sense, however, because there may be small-scale irregularities of the laser beam or target within the focal spot and thus the source size may be determined by this scale length. The magnetic field generated by such small-scale fluctuations is rapidly changing its sign and hence may not influence the overall transport process and dynamic motion. But we show that this microfluctuation leads to a long-scale magnetic field through the "dynamo" effect⁹ and that the amplitude of the magnetic field generated by this mechanism can be greater than that caused by the thermoelectric effect of long scale length. Furthermore, we discuss an experiment which implies the realization of this mechanism.

First, let us estimate the amplitude of the magnetic field generated by the dynamo effect, using a configuration shown in Fig. 1. This figure illustrates the ablation layer, and hence the density gradient is antiparallel to the temperature gradient in the x direction. Furthermore, the temperature has a slow variation in the y direction due to the finite focal-spot size of the incident energy and so on. The density fluctuation in the y direction may originate from target irregular-

ities and may be a rapidly varying function of y with the wave number k . Consequently, we can set

$$n(x, y) = n_0(x, y) [1 + \delta \sin(ky)],$$

$$T(x, y) = T_0(x, y),$$

where $n_0(x, y)$ and $T_0(x, y)$ are slowly varying functions with respect to their arguments x and y . For simplicity, constant pressure along the x direction is assumed, and hence $n_0 \propto \exp(-x/L')$ and $T_0 \propto \exp(x/L')$ are assumed with the assumption $kL' \gg 1$.

The motion induced by this configuration is estimated to be

$$\begin{aligned} v_x &= 0, \\ v_y &= -(C_{\infty}^2/v_0) \delta k L' \cos(ky) [1 - \exp(-\sigma_1 t)], \end{aligned} \quad (1)$$

where $\sigma_1 = v_0/L'$, if n and T remain constant in time and the terms of the order of $(kL')^{-1}$ are neglected compared with unity. Here v_0 is the uniform convection velocity in the x direction. In this configuration, a magnetic field is also generated according to

$$\frac{\partial B_z}{\partial t} = -\nabla \cdot (\vec{v} B_z) + \frac{c}{ne} (\nabla T \times \nabla n)_z + \nabla D_E \nabla B_z, \quad (2)$$

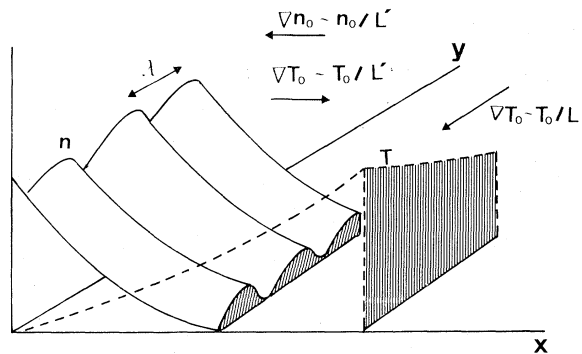


FIG. 1. Schematic of the configuration used in the analysis. The target has rippling structure along the y direction.

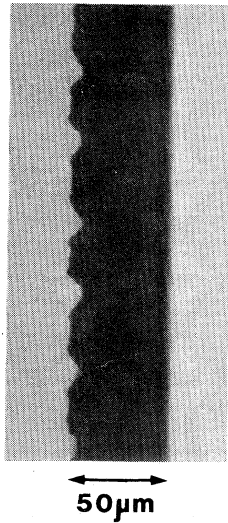


FIG. 2. Cross-sectional view of the rippled copper target used in the experiment.

where D_B is the diffusion coefficient. Retaining leading order terms, we integrate Eq. (2) as

$$B_z = (cT_0/eL'\sigma_2)\delta k \cos(ky)[1 - \exp(-\sigma_2 t)]; \quad (3)$$

$$\sigma_2 = v_0/L' + k^2 D_B.$$

Since v_y and B_z are in the same phase with respect to y , the spatial average of the product $v_y B_z$ along the y direction becomes a slowly varying function of y . Here, this dynamo term can generate a long-scale magnetic field \bar{B}_z such as

$$\frac{\partial \bar{B}_z}{\partial t} = \frac{\delta^2 k^2 c}{2v_0 e \sigma_2} [1 - \exp(-\sigma_1 t)] \times [1 - \exp(-\sigma_2 t)] \frac{\partial T_0 C_{s0}}{\partial y} \equiv S_{BD}. \quad (4)$$

If the characteristic scale length of temperature in the y direction is L , we can estimate the other source term of the long-scale magnetic field, i.e., the thermoelectric effect,

$$\frac{\partial \bar{B}_z}{\partial t} = -\frac{c}{n_0 e} \frac{\partial T_0}{\partial y} \frac{\partial n_0}{\partial x} = -\frac{c T_0}{e L L'} \equiv S_{BT}. \quad (5)$$

It may be useful to compare the magnitudes of these sources in the limit of $t \rightarrow \infty$:

$$S_{BD}/S_{BT} = (\delta k L' C_{s0}/v_0)^2 / (1 + k^2 D_B L'/v_0). \quad (6)$$

If we assume that the flow is almost sonic ($v_0/C_{s0} \sim 1$) and $\delta \sim O(1)$, the necessary condition for the ratio [Eq. (6)] being greater than unity becomes

$$k L' > 1, \quad (7)$$

$$D_B/L' C_{s0} = 8.3(AZ)^{1/2}/T_e v^2 L' < 1, \quad (7')$$

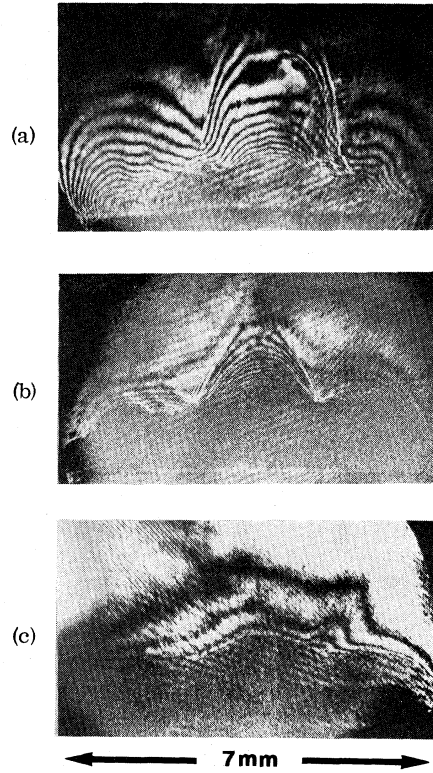


FIG. 3. Density profiles at 200 ns for (a) $\lambda = 40 \mu\text{m}$, (b) $\lambda = 200 \mu\text{m}$, and (c) flat target. The larger the deformation of the blowoff plasma front becomes, the shorter the rippling wavelength is.

where A and Z_e are the mass number and ionic charge of the material. These conditions are accessible and hence the dynamo effect can become greater than the thermoelectric effect in the typical conditions of inertial confinement fusion.

Next, we describe an experiment¹⁰ which may imply this dynamo effect. A carbon-dioxide (CO_2) laser of 1-kJ, 50-ns pulse and 230 mm in diameter driven by an electron-beam-controlled oscillator LEKKO I (unstable mode) is linearly polarized in the TEM_{00} mode and focused normally on a $7 \times 7\text{-mm}^2$ target to a 3-mm spot by an $R = 4$ m mirror. The 50- μm -thick copper foil target was ruled at period λ with a yttrium-aluminum-garnet laser, as shown in Fig. 2. A three-channel holographic interferometer using a 2-ns ruby laser measures ablating plasma profiles perpendicular to the CO_2 -laser axis. The laser polarity is parallel to the surface of the page in Fig. 2. Figure 3 shows the density profile at 200 ns after

the CO₂-laser pulse rise for various periods λ , where one fringe corresponds to $4 \times 10^{17} \text{ cm}^{-3}$. The plasma blows are strong in the laser cone angle, resulting in three peaks and two nodes. For $\lambda = 40 \text{ } \mu\text{m}$, a strong deformation of the blow-off plasma is observed. On the other hand, it is not clear in a flat target. As the period becomes longer ($\lambda = 200 \text{ } \mu\text{m}$), the deformation becomes weaker.

Theoretically, the magnitude of the long-scale magnetic field \bar{B}_z can be obtained from Eq. (4) as

$$\beta = \bar{B}_z / (4\pi n_0 T_0)^{1/2} \sim \delta^2 k^2 v_{Te} C_{s0}^2 t^3 / 3\omega_{pe} L L' \\ \sim 0.9 Z T_{eV}^{3/2} t_{ns}^3 / A L_{mm} L'_{mm} \lambda_{\mu m}^2.$$

The condition $\beta \sim 1$ is attained for $t > t_c$, where t_c is about 900 ps for $\lambda = 40 \text{ } \mu\text{m}$ and 2.7 ns for $\lambda = 200 \text{ } \mu\text{m}$ if f is set to 0.1.¹¹ This means that the magnetic field can grow to a value which is enough to influence plasma motion within a short time compared with the laser pulse width. Consequently, the amplitude of the generated magnetic field \bar{B}_z is inversely proportional to λ^2 and this qualitatively agrees with the experimental results, if the deformation of the plasma flow observed in our experiment is due to this long-scale magnetic field.

In the experimental condition, the temperature is estimated to be about 200–600 eV for a flux limitation factor $f = 0.6$ –0.1 from absorbed intensity 10^{11} W/cm^2 and hence the criteria Eqs. (7) and (7') for the scale length L' become $L' > \max(174 f^{4/3} \text{ } \mu\text{m}, k^{-1})$ for a copper target ($A = 63$ and $Z \sim 20$). The scale length L' may be estimated by a steady ablation structure where convection loss balances heat conduction,¹² i.e., $C_{s0} \partial T / \partial x \sim (v_{Te} L_{Te}) \partial^2 T / \partial x^2$. Consequently, $L' \sim (m_i / Z m_e)^{1/2} L_{Te} \sim 42.9 (A/Z)^{1/2} L_{Te}$, where v_{Te} is the electron thermal velocity and L_{Te} is the electron mean free path; $L_{Te} \sim 1.5 \times 10^{-7} T_{eV}^2 / (Z n_e / 10^{19}) \text{ cm}$. In our experiment, L' is estimated to be about 2 mm for $f = 0.1$ and the above criteria are satisfied; hence the dynamo effect dominates over the thermoelectric effect.

In summary, we have proposed a new mechanism of long-scale magnetic field generation. This mechanism originates from small-scale fluctuations of the target surface or the laser

beam, and the dynamo effect of such small-scale fluctuations leads to a long-scale magnetic field. The criteria for our proposed mechanism to dominate over the thermoelectric effect were given and were shown to be accessible in present day experiments.

A part of this work was done when one of the authors (T.Y.) was visiting the Institute for Fusion Studies, University of Texas at Austin. He would like to thank Dr. T. Tajima and Dr. F. Brunel for helpful discussions and Professor M. N. Rosenbluth for hospitality. The authors are indebted to the Ministry of Education of Japan for the funding of the Japan-U.S. coordination of fusion research.

¹S. P. Obenschain, J. Grun, B. H. Ripin, and E. A. McLean, *Phys. Rev. Lett.* **46**, 1402 (1981).

²H. Shiraga, T. Mochizuki, S. Sakabe, K. Okada, A. Kikuchi, and C. Yamanaka, *Phys. Rev. Lett.* **49**, 1244 (1982).

³G. Taylor, *Proc. Roy. Soc. London, Ser. A* **201**, 192 (1930).

⁴R. L. McCrory, L. Montierth, R. L. Morse, and C. P. Verdon, *Phys. Rev. Lett.* **46**, 336 (1981); M. H. Emery, J. H. Gardner, and J. P. Boris, *Phys. Rev. Lett.* **48**, 677 (1982).

⁵K. Fong and B. Ahlborn, *Phys. Fluids* **22**, 416 (1979); J. H. Gardner, D. L. Book, and I. B. Bernstein, *J. Fluid Mech.* **114**, 49 (1982).

⁶T. Yabe, A. Nishiguchi, and N. Ueda, *Appl. Phys. Lett.* **39**, 222 (1981); T. Yabe *et al.*, in *Laser Interaction and Related Plasma Phenomena* (Plenum, New York, 1983), Vol 6.

⁷T. Yabe, K. Mima, T. Sugiyama, and S. Yoshikawa, *Phys. Rev. Lett.* **48**, 242 (1982), and references therein.

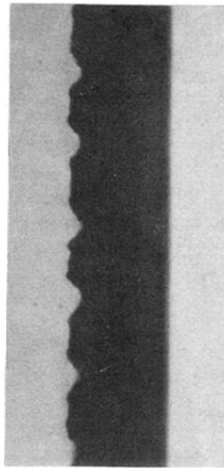
⁸J. A. Stamper, K. Papadopoulos, R. N. Sudan, S. O. Dean, E. A. McLean, and J. M. Dawson, *Phys. Rev. Lett.* **26**, 1012 (1971); Y. Kitagawa, Aye Thein, Y. Yamada, M. Yokoyama, and C. Yamanaka, *J. Appl. Phys.* **50**, 5206 (1979).

⁹E. A. Witalis, in *Laser Interaction and Related Plasma Phenomena*, edited by H. Schwarz and H. Hora (Plenum, New York, 1974), Vol. 3A, p. 237.

¹⁰Y. Kitagawa *et al.*, Annual Progress Report on Laser Fusion Program, Institute of Laser Engineering, Osaka University, Report No. ILE-APR-79, 1981 (unpublished), p. 209.

¹¹A. R. Bell, R. G. Evans, and D. J. Nicholas, *Phys. Rev. Lett.* **46**, 243 (1981).

¹²J. L. Bobin, *Phys. Fluids* **14**, 2341 (1971).



50 μ m

FIG. 2. Cross-sectional view of the rippled copper target used in the experiment.

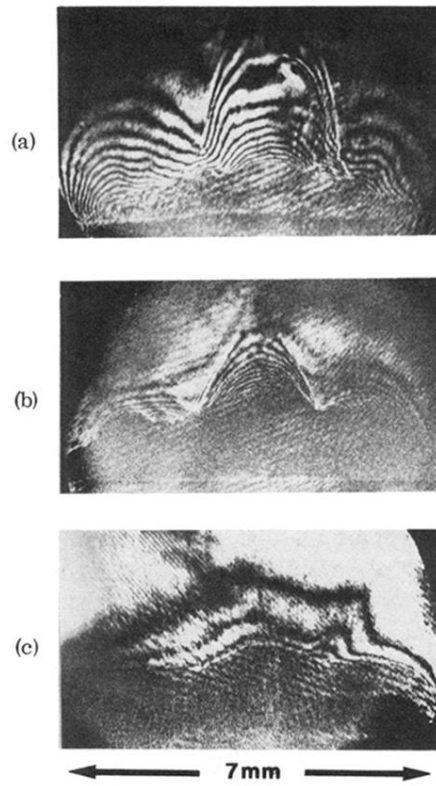


FIG. 3. Density profiles at 200 ns for (a) $\lambda = 40 \mu\text{m}$, (b) $\lambda = 200 \mu\text{m}$, and (c) flat target. The larger the deformation of the blowoff plasma front becomes, the shorter the rippling wavelength is.